

# Style for IFAC Conferences & Symposia: Use Title Case for Paper Title

Alessandra Elisa Sindi Morando <sup>\*,\*\*</sup> Jossué Cariño <sup>\*\*</sup>  
Pedro Castillo <sup>\*\*</sup> Roberto Sacile <sup>\*</sup> Enrico Zero <sup>\*</sup>

<sup>\*</sup> University of Genoa, Genoa, Italy  
*alessandra.elisa.sindi.morando@edu.unige.it, roberto.sacile@unige.it,*  
*enrico.zero@dibris.unige.it*  
<sup>\*\*</sup> Université de technologie de Compiègne, CNRS, Heudiasyc,  
Compiègne, France  
*alessandra-elisa-sindi.morando@utc.fr, {jossue.escobar,*  
*pedro.castillo}@hds.utc.fr*

---

**Abstract:** ...

**Keywords:** ...

---

## 1. INTRODUCTION

Multi-agent systems (MASs) are nowadays used in a variety of applications from as they can perform complex tasks, which would otherwise impossible for a single robot. This is even more the case when considering heterogeneous fleet where the strengths of one type of robot can compensate for the limitations of another. For example, to monitor a large area, multiple ground agents can move from one point to another being supervised from above by a drone with a wide field of view. To deepen the subject and understand both the potential tasks and challenges of MASs, the reader can refer to the work of Maldonado et al. (2024).

One of the fundamental cooperative tasks when working with multi-agents is formation control. This topic has been studied for years. For example, already Lee and Chong (2009) already proposed a decentralized control algorithm for a team of two-wheeled robots to achieve achieve a geometric pattern. However, formation control remains an hot challenging topic to this day. Tran et al. (2021) experimentally validated a robust distributed control based on negative imaginary systems consensus theory, using both ground robots and an air-ground fleet. In the work of Güler and İsa E. Yıldırım (2023), each agent computes its control action in a leader-follower manner using local extended Kalman filter's estimates to achieve a desired shape together with other wheeled robots and a drone. An optimal distributed formation control algorithm for double-integrator multi-agents has been presented and validated through simulations by Huang et al. (2023). Aditya and Werner (2023) defined the formation problem for a group of double-integrator agents as a discrete-time game whose solution is given by a state-dependent Riccati equation. A robust distributed consensus controller is presented by Restrepo et al. (2023) to address the rendezvous problem and applied in simulation to a swarm of drones. In the recent years, reinforcement learning has used in many areas including formation control. Wang et al. (2020) addressed multi-particle formation control by combining

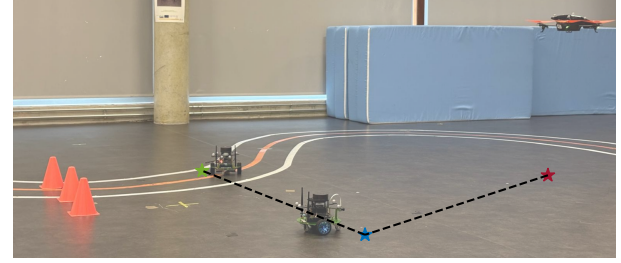


Fig. 1. This paper proposes a formation control for a heterogeneous fleet to attain a desired shape despite obstacles.

graph attention networks and multiple long short-term memories to achieve the desired shape and avoid collisions respectively. A position and an orientation robust controllers based on reinforcement learning are proposed and validated through simulations by Zhong et al. (2025) for the formation of a term of quadrotors.

In this context is placed this work which proposes a novel formation control scheme for a team consisting of a quadcopter and two unicycles, as show in Fig. 1. When addressing the multi-agent formation, there are two main challenges to solve: achieving the desired shape and avoiding collisions. On one hand, for the first challenge, a distributed controller combining Feedback Linearization (FL) and an optimal linear controller based on Linear Matrix Inequalities (LMIs) is presented. LMIs are a powerful mathematical tool used in many applications among which also formation control. In the work of Trejo et al. (2023), an LMI is solved to design the controller and observer gains, guaranteeing stable formation flight for a group of quadcopters. Deshpande et al. (2011) propose a formation control with artificial fixed delays for multiple double-integrators and verify the asymptotic stability of the scheme by checking the solvability of an LMI. Semsar-Kazerooni and Khorasani (2009) present an LMI formulation of the LQR problem to guarantee stable state consensus with an optimal control effort in a multi-agent system.

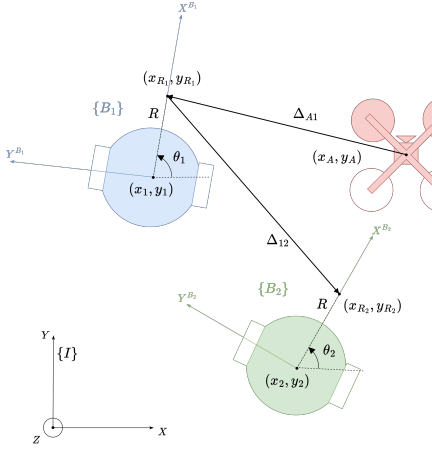


Fig. 2. Air-ground heterogeneous fleet.

On the other end, to avoid collision avoidance, the chosen solution is Artificial Potential Field (APF). In analogy with a particle moving in an electrostatic or gravitational field, virtual repulsive force fields are simulated to ward off the robot from an obstacle. This approach has been widely used in formation control of ground vehicles, see for example the work of Yongshen et al. (2018). However, in more recent works, e.g. Han et al. (2024) and Piet et al. (2025), APFs are employed to navigate around obstacles and prevent collisions while attaining the desired shape.

This paper represents the continuation of the previous work by Morando et al. (2025), where a control architecture combining Feedback Linearization (FL), a robust LMI-based controller and APFs was proposed and validated through simulations for the formation of three unicycles. The successive developments sought to manage the challenge of a heterogeneous team (replacing a ground vehicle with a quadcopter) by adapting the methodology and then experimentally validating the new solution. The contributions of this work are: a) a controller involving FL, a LMI-based controller and APFs is presented for the stable formation of an air-ground fleet; b) the proposed controller has been validated through MATLAB Simulink simulations and a comprehensive set of experiments in an indoor arena, including both static and dynamic obstacle scenarios. The remainder paper is structured as follows. In Section 2, the mathematical model used to describe the team is stated. The proposed formation controller is detailed in Section 3. The simulations and the experiments results are reported and analyzed in Section 4 and in Section 5 respectively. Finally, conclusions are drawn in Section 6.

## 2. HETEROGENEOUS FLEET MODELING

In this section, the dynamics of the agents composing the team (i.e., of the two unicycles and the quadrotor, as shown in Fig. 2.) are described and adapted to then apply the LMI approach. The well-known kinematic model of a two-wheeled ground robot  $G_i$  is

$$\begin{cases} \dot{x}_i = v_i \cos \theta_i \\ \dot{y}_i = v_i \sin \theta_i \\ \dot{\theta}_i = \omega_i \end{cases} \quad (1)$$

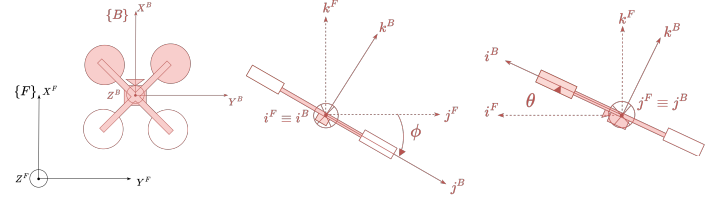


Fig. 3. Quadcopter's roll  $\phi$  and pitch  $\theta$  angles.

where  $(x_i, y_i, \theta_i)$  is the pose of the agent and  $(v_i, \omega_i)$  are the linear and angular velocities respectively. The equations (1) describing the motion of the center of rotation are non-linear. But still, if a point located at distance  $R > 0$  from  $(x_i, y_i)$  denote as  $(x_{R_i}, y_{R_i})$ , is considered and new virtual inputs are defined  $(u_{i,x}, u_{i,y})$ , the dynamics become linear:

$$\begin{cases} \dot{x}_{R_i} = u_{i,x} \\ \dot{y}_{R_i} = u_{i,y} \end{cases} \quad (2)$$

Moving on to the drone, as in the formation problem deals with the  $(X, Y)$ -dynamics, some simplifying hypothesis have been made. First, let us assume that there is an inner attitude controller. Hence, the focus is only on the translational dynamics which are:

$$\begin{cases} m\ddot{x}_A^F = -T \sin \theta \\ m\ddot{y}_A^F = T \cos \theta \sin \phi \\ m\ddot{z}_A^F = T \cos \theta \cos \phi - mg \end{cases} \quad (3)$$

Let analyze the equations with the help of Fig. 3. The state  $(x_A^F, y_A^F, z_A^F)$  represents the position of the drone w.r.t. the inertial frame  $\{F\}$ . The frame  $\{F\}$  has been used instead of  $\{I\}$  to be aligned with the framework employed to implement the controller for the drone, see Section 5. The angles  $\phi$  and  $\theta$  are the roll and pitch Euler angles of the body frame  $\{B\}$  (fixed to the drone) relative to the inertial frame  $\{F\}$ . Ignoring the small body forces, the only forces acting on the drone are the thrust produced by the motors  $T$  along the  $k^B$  direction and the gravity  $mg$  along the  $-k^F$  direction. Let suppose that the  $Z$ -controller

$$T = (r_1 + mg)/(\cos \phi \cos \theta) \quad (4)$$

is such that the drone's mass is compensated in a short time by  $r_1$ , i.e.  $r_1 \rightarrow 0$ . This implies that the  $(x, y)$ -dynamics will not include the mass of the drone, as the  $Z$ -controller already compensated it. Finally, let us make the hypothesis that the roll and pitch angles are small, i.e.  $\phi, \theta \approx 0$ . Then, the translational dynamics simplify to

$$\begin{cases} \ddot{x}_A^F = -g\theta \\ \ddot{y}_A^F = g\phi \end{cases} \quad (5)$$

At this point, all the agents can be described by the linear models (1) and (5). To define the formation problem, let us introduce the quantities

$$\Delta_{A1} = [\Delta_{A1,x} \ \Delta_{A1,y}]^T \quad (6a)$$

$$\Delta_{A1,x} = x_{R_1} - x_A = x_{R_1} - y_A^F \quad (6b)$$

$$\Delta_{A1,y} = y_{R_1} - y_A = y_{R_1} - x_A^F \quad (6c)$$

with  $(x_A, y_A)$  the position of the drone w.r.t the inertial frame  $\{I\}$ ,

$$\Delta_{12} = [\Delta_{12,x} \ \Delta_{12,y}]^T \quad (7a)$$

$$\Delta_{12,x} = x_{R_2} - x_{R_1}, \ \Delta_{12,y} = y_{R_2} - y_{R_1} \quad (7b)$$

the desired inter-distances  $\Delta_{A1}^d$  and  $\Delta_{12}^d$ , and the desired position of the drone  $(x_A^d, y_A^d)$  w.r.t the inertial frame

$\{I\}$  (constant over time). The overall dynamics of the formation's errors are as follows

$$\begin{cases} \ddot{e}_{A,x} = -g\theta \\ \ddot{e}_{A,y} = g\phi \\ \dot{e}_{\Delta_{A1,x}} = u_{1,x} - \dot{e}_{A,y} \\ \dot{e}_{\Delta_{A1,y}} = u_{1,y} - \dot{e}_{A,x} \\ \dot{e}_{\Delta_{12,x}} = u_{2,x} - u_{1,x} \\ \dot{e}_{\Delta_{12,y}} = u_{2,y} - u_{1,y} \end{cases} \quad (8)$$

with

$$e_{A,x} = x_A^F - y_A^d, e_{A,y} = y_A^F - x_A^d \quad (9)$$

$$e_{\Delta_{A1,x}} = \Delta_{A1,x} - \Delta_{A1,x}^d, e_{\Delta_{A1,y}} = \Delta_{A1,y} - \Delta_{A1,y}^d \quad (10)$$

$$e_{\Delta_{12,x}} = \Delta_{12,x} - \Delta_{12,x}^d, e_{\Delta_{12,y}} = \Delta_{12,y} - \Delta_{12,y}^d \quad (11)$$

Let us define the state and control vectors as follows

$$\mathbf{e}^T = [e_{A,x} \ \dot{e}_{A,x} \ e_{A,y} \ \dot{e}_{A,y} \ e_{\Delta_{A1,x}} \ e_{\Delta_{A1,y}} \ e_{\Delta_{12,x}} \ e_{\Delta_{12,y}}] \quad (12a)$$

$$\mathbf{u}_A = \begin{bmatrix} \phi \\ \theta \end{bmatrix}, \mathbf{u}_1 = \begin{bmatrix} u_{1,x} \\ u_{1,y} \end{bmatrix}, \mathbf{u}_2 = \begin{bmatrix} u_{2,x} \\ u_{2,y} \end{bmatrix}, \mathbf{u} = \begin{bmatrix} \mathbf{u}_A \\ \mathbf{u}_1 \\ \mathbf{u}_2 \end{bmatrix} \quad (12b)$$

Hence, the heterogeneous fleet's dynamics can be written in a matrix form:

$$\dot{\mathbf{e}} = A\mathbf{e} + B\mathbf{u} \quad (13)$$

By discretizing with sampling time  $\Delta T$  using the Euler method:

$$\mathbf{e}(k+1) = A_d\mathbf{e}(k) + B_d\mathbf{u}(k) \quad (14)$$

with  $A_d = I + \Delta T A$  and  $B_d = \Delta T B$ . To model real-world disturbances, it is assumed that an additive zero-mean disturbance  $\mathbf{d}(k)$  is acting on the input channel, i.e.

$$\mathbf{e}(k+1) = A_d\mathbf{e}(k) + B_d\mathbf{u}(k) + B_d\mathbf{d}(k) \quad (15)$$

Let us make the following hypothesis: a) the drone knows its position; b) the robot  $G_1$  knows its position w.r.t the quadcopter; c) the robot  $G_2$  knows its position w.r.t the other agent  $G_1$ ; d) all unicycles are aware of their distance from any obstacles on the ground; e) a hierarchy is defined between the ground robots:  $G_1$  has the priority over  $G_2$ .

### 3. FORMATION CONTROLLER

This section aims to detail the proposed formation controller. The two crucial issues, formation maintenance and collision avoidance, are addressed respectively in the next two subsections.

#### 3.1 Formation Maintenance: an LMI Approach

The first goal is to ensure the robots achieve the desired shape while using only local measurements and counter-acting the worst-case disturbance. Based on the previous hypotheses, the measurements of each agent are as follows:

$$\mathbf{z}_A = \begin{bmatrix} e_{A,x} \\ e_{A,y} \\ \dot{e}_{A,x} \\ \dot{e}_{A,y} \end{bmatrix} = C_A \mathbf{e} \quad (16a)$$

$$\mathbf{z}_1 = \begin{bmatrix} e_{\Delta_{A1,x}} \\ e_{\Delta_{A1,y}} \end{bmatrix} = C_1 \mathbf{e}, \mathbf{z}_2 = \begin{bmatrix} e_{\Delta_{12,x}} \\ e_{\Delta_{12,y}} \end{bmatrix} = C_2 \mathbf{e} \quad (16b)$$

with  $C_A$ ,  $C_1$ , and  $C_2$  the measurement matrices of the three. The idea is to formulate the robust formation control problem as a dynamic game between two players: one is the control action and the other opponent is the "nature". In the proposed solution, at each time step  $k$

the control action to be applied at the next step  $\mathbf{u}(k)$  is obtained by solving the following min-max problem defined over a one-step horizon.

$$\begin{aligned} \min_{\mathbf{u}(k)} \max_{\mathbf{e}(k) \neq 0} & \frac{J(k)}{\|\mathbf{e}(k)\|_2^2} \\ \text{s.t. } & \mathbf{z}_i(k) = C_i \mathbf{e}(k) \\ & \mathbf{u}_i(k) = \boldsymbol{\mu}_i(\mathbf{z}_i(k)) \quad i \in \{A, 1, 2\} \end{aligned} \quad (17)$$

with

$$J(k) = \mathbf{u}(k)^T Q_u \mathbf{u}(k) + \mathbf{e}(k+1)^T Q_e \mathbf{e}(k+1) + \mathbf{e}(k)^T Q_e \mathbf{e}(k) \quad (18)$$

The cost function can be rewritten by substituting the evolution model equation (15).

$$J(k) = \begin{bmatrix} \mathbf{e}(k) \\ \mathbf{u}(k) \end{bmatrix}^T \begin{bmatrix} Q_e + A_d^T Q_e A_d & A_d^T Q_e B_d \\ B_d^T Q_e A_d & Q_u + B_d^T Q_e B_d \end{bmatrix} \begin{bmatrix} \mathbf{e}(k) \\ \mathbf{u}(k) \end{bmatrix} \quad (19)$$

Hence, the min-max problem to be solved is

$$\begin{aligned} \min_{\mathbf{u}(k)} \max_{\mathbf{e}(k) \neq 0} & \frac{\begin{bmatrix} \mathbf{e}(k) \\ \mathbf{u}(k) \end{bmatrix}^T \begin{bmatrix} Q_{ee} & Q_{eu} \\ Q_{ue} & Q_{uu} \end{bmatrix} \begin{bmatrix} \mathbf{e}(k) \\ \mathbf{u}(k) \end{bmatrix}}{\|\mathbf{e}(k)\|_2^2} \\ \text{s.t. } & \mathbf{z}_i(k) = C_i \mathbf{e}(k) \\ & \mathbf{u}_i(k) = \boldsymbol{\mu}_i(\mathbf{z}_i(k)) \quad i \in \{A, 1, 2\} \end{aligned} \quad (20)$$

with

$$Q_{ee} = Q_e + A_d^T Q_e A_d \quad (21)$$

$$Q_{eu} = A_d^T Q_e B_d, Q_{ue} = Q_{eu}^T \quad (22)$$

$$Q_{uu} = Q_u + B_d^T Q_e B_d \quad (23)$$

Note that the problem (20) has the same form as the one considered by Gattami et al. (2012) in their paper where they prove that the linear policy is optimal, i.e.

$$\mathbf{u}_i^*(k) = K_i^* \mathbf{z}_i(k) \quad i \in \{A, 1, 2\} \quad (24)$$

where the matrices  $K_i^*$  can be obtained by solving the following LMI:

$$\begin{aligned} \min_{\gamma, K} & \gamma \\ \text{s.t. } & K = \text{diag}(K_A, K_1, K_2) \\ & \begin{pmatrix} Q_{ee} - \gamma I + Q_{eu} K C + C^T K^T Q_{eu}^T & C^T K^T \\ K C & -Q_{uu}^{-1} \end{pmatrix} \leq 0 \end{aligned} \quad (25)$$

#### 3.2 Obstacle Avoidance: APFs

Collisions can still occur when the agents attain the desired shape. Moreover, obstacles can be present in the robots' way. It is therefore crucial to propose a solution to avoid crashes for the experimental validation. This is where APFs come to help. For simplicity, let us consider at first a scenario where the ground is clean and collisions may occur between  $G_1$  and  $G_2$ . On one hand, since  $G_1$  has the highest priority, there is no need to correct the control action  $\mathbf{u}_1^*(k)$ . On the other hand, the robot  $G_2$  has to correct its way to avoid the other ground vehicle. A repulsive force can be used to attain this, with a direction opposite to the vector going from  $G_2$  to  $G_1$  and a magnitude as follows:

$$|F_{12}| = \begin{cases} \left( k_{Rep}/d_{Rep} \right)^2 \left[ (1/d_{12}) - (1/d_{Rep}) \right] & d_{12} < d_{Rep} \\ 0 & d_{12} \geq d_{Rep} \end{cases} \quad (26)$$

with  $d_{12} = \sqrt{\Delta_{12,x}^2 + \Delta_{12,y}^2}$  and  $d_{Rep}$  the distance after which the robot is not influenced by the obstacle. The final control inputs for  $G_2$  are:

$$\begin{aligned} u_{2,x}(k) &= u_{2,x}^*(k) + \frac{1}{2} \frac{F_{12,x}(k)}{M} \Delta T \\ u_{2,y}(k) &= u_{2,y}^*(k) + \frac{1}{2} \frac{F_{12,y}(k)}{M} \Delta T \end{aligned} \quad (27)$$

with  $M$  the two-wheeled robots mass. The same approach can be extended to a scenario with both static and dynamic obstacles. Suppose that there are  $N$  (static or dynamic) obstacles, then the final control inputs for both unicycles are:

$$\begin{aligned} u_{1,x}(k) &= u_{1,x}^*(k) + \frac{1}{2} \frac{\sum_{j=1}^N F_{j1,x}(k)}{M} \Delta T \\ u_{1,y}(k) &= u_{1,y}^*(k) + \frac{1}{2} \frac{\sum_{j=1}^N F_{j1,y}(k)}{M} \Delta T \\ u_{2,x}(k) &= u_{2,x}^*(k) + \frac{1}{2} \frac{F_{12,x}(k) + \sum_{j=1}^N F_{j2,x}(k)}{M} \Delta T \\ u_{2,y}(k) &= u_{2,y}^*(k) + \frac{1}{2} \frac{F_{12,y}(k) + \sum_{j=1}^N F_{j2,y}(k)}{M} \Delta T \end{aligned} \quad (28)$$

#### 4. SIMULATIONS RESULTS

The first validation of the proposed formation controller has been done via simulations in MATLAB R2022a Simulink. To choose the parameters, the target robots' characteristics have been taken into account from the beginning in the tuning phase. Two Waveshare JetBot Pro ROS AI and a Parrot AR.Drone 2.0 compose the experimental equipment specifically, see Section 5. First, both the linear and the angular velocities of the ground vehicles have been limited:  $|v_i| \leq 0.5 \text{ m s}^{-1}$  and  $|\omega_i| \leq 0.5 \text{ rad s}^{-1}$ . Concerning the distance of the point from the center of rotation, it has been chosen  $R = 0.18 \text{ m}$ . The continuous-time models have been discretized with  $\Delta T = 0.02 \text{ s}$ . The weighting matrices used in the definition of the LMI have been set to  $Q_e = 2e4 I_{8 \times 8}$  and  $Q_u = \text{blkdiag}(0.01 I_{2 \times 2}, 0.04 I_{4 \times 4})$ . The obtained  $K_i^*$  were

$$K_A^* = \begin{bmatrix} 0 & -0.0770 & 0 & -1.2440 \\ 0.0770 & 0 & 1.2440 & 0 \end{bmatrix} \quad (29)$$

$$K_1^* = \begin{bmatrix} -9.6717 & 0 \\ 0 & -9.6717 \end{bmatrix} \quad (30)$$

$$K_2^* = \begin{bmatrix} -15.0765 & 0 \\ 0 & -15.0765 \end{bmatrix} \quad (31)$$

which implies in closed loop the following eigenvalues of the closed-loop system

$$p = \text{eig}(A_d + B_d K^* C) = \begin{cases} 0.6985 & \mu = 2 \\ 0.7572 & \mu = 2 \\ 0.8066 & \mu = 2 \\ 0.9988 & \mu = 2 \end{cases} \quad (32)$$

which are all inside the unitary circle, check Fig. 4. Moving to the APFs, the mass of the Jetbot's robot is  $M = 1.4 \text{ kg}$

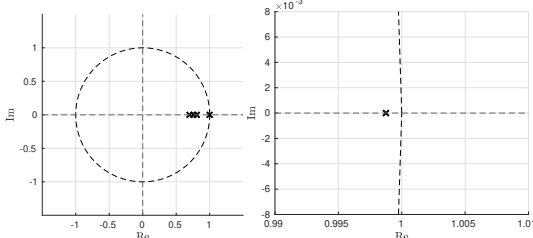


Fig. 4. Poles of the closed-loop system in the imaginary plane

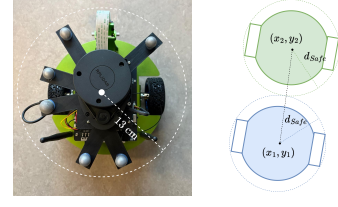


Fig. 5. The physical robot is contained entirely in a circle of radius  $d_{Safe} = 0.13 \text{ m}$ . Consequently, if the centers of rotation are at a distance less than  $2d_{Safe}$  it means that the agents collided.

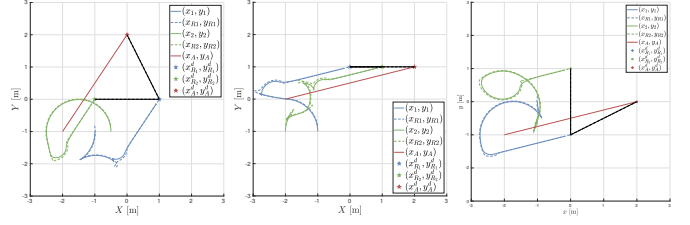


Fig. 6. Trajectories of the three agents with desired and actual interdistances in ideal simulations.

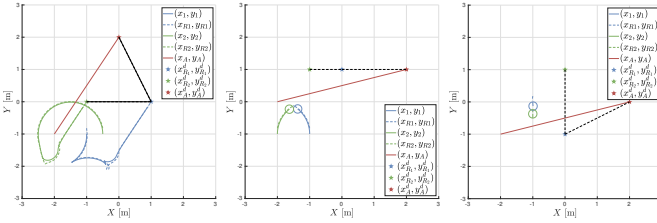
and it has been chosen  $k_{Rep} = 700$  and  $d_{Rep} = 5R$ . In the simulations, the unicycles are treated as mass points but nevertheless the objective is to verify if the physical robots will crash. For this reason, the robots are considered to have collided in the simulation if  $d_{12} \leq 2d_{Safe}$  (with  $d_{Safe} = 0.13 \text{ m}$ , see Fig. 5). For a quantitative analysis, the time required for the agents to reach the formation was studied. Let us define the key performance index  $\bar{t}$  as follows:

$$\forall t \geq \bar{t} : \begin{cases} |e_{A,x}(t)| < \varepsilon, |e_{A,y}(t)| < \varepsilon \\ |e_{\Delta_{A1,x}}(t)| < \varepsilon, |e_{\Delta_{A1,y}}(t)| < \varepsilon \\ |e_{\Delta_{12,x}}(t)| < \varepsilon, |e_{\Delta_{12,y}}(t)| < \varepsilon \end{cases} \quad (33)$$

with  $\varepsilon$  a negligible error. For the simulations, it has been set  $\varepsilon = 0.10 \text{ m}$ .

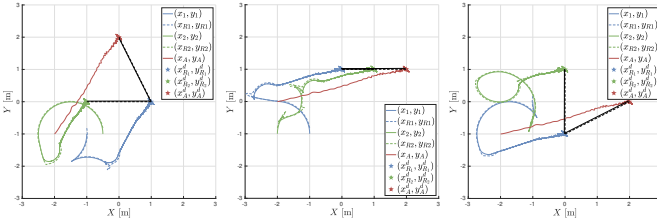
The first set of simulations considers a scenario with the ground clean and without disturbances, i.e.  $\mathbf{d}(k) = 0$ . The results are shown in Fig. 6. For each unicycle, they are plotted the 2D-trajectories of the center of rotation and of the point  $(x_{R_i}, y_{R_i})$  with a solid and a dotted line respectively. The desired inter distances drone- $G_1$  and  $G_1-G_2$  are plotted with solid black, while the actual inter distances at the end of the simulation are the dotted black lines. Finally, stars denote the desired final positions of the robots based on the definitions of  $(x_A^d, y_A^d)$ ,  $\Delta_{A1}^d$  and  $\Delta_{12}^d$ . From Fig. 6, it is straightforward to conclude that the agents make the formation avoiding collisions in all scenarios, which differ in initial conditions and desired geometric shapes. The key performance index for the first scenario is  $\bar{t} = 54.76 \text{ s}$ , for the second case  $\bar{t} = 59.38 \text{ s}$ , and for the last case  $\bar{t} = 59.38 \text{ s}$ .

To demonstrate the importance of APFs, the simulations have been redone without repulsive forces. If a collision occurs this time, the ground vehicles will halt and remain stopped until the end of the test. Fig. 7 displays the resulting trajectories. In the first case, the curves are the same as Fig. 6a since the unicycles do not clash. However, the differences are obvious in the other two cases: compare



(a) Triangle Top      (b) Line Segment      (c) Triangle Right

Fig. 7. Trajectories of the three agents without APF in ideal simulations.



(a) Triangle Top      (b) Line Segment      (c) Triangle Right

Fig. 8. Trajectories of the three agents with desired and actual interdistances in simulation with disturbances.

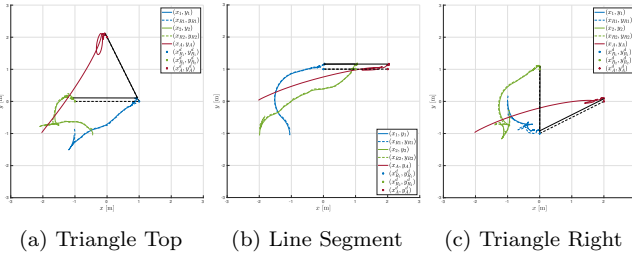


Fig. 9. Trajectories of the three agents with desired and actual interdistances in the experiments.

Fig. 7b and Fig. 7c with Fig. 6b and Fig. 6c. It is clear that without APF, the unicycles get too close and they must stop. Hence, even if the drone reaches the desired position  $(x_A^d, y_A^d)$ , the overall formation is not attained by the fleet. On the opposite, thanks to the artificial repulsive forces the robot  $G_2$  deviates its path to stay at a safe distance from  $G_1$ .

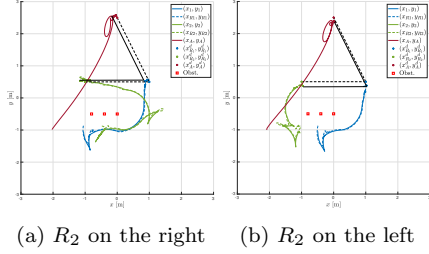
The last set of simulations aims to study the robustness of the proposed control scheme in the presence of the zero-mean disturbance  $\mathbf{d}(k)$ . The disturbance has been modeled in particular as a gaussian noise with variance  $\Sigma = 0.1I_{6 \times 6}$ . The results are presented in Fig. 8. The trajectories are similar to the ones in Fig. 6, but the agents in the end oscillate around the desired final positions due to disturbance  $\mathbf{d}(k)$  (though they remain within a small neighborhood). This is the same reason why the solid and dotted lines do not exactly overlap: the dotted shape appears to be a translated version of the solid one. However, collisions between  $G_1$  and  $G_2$  are avoided and the formation is reached after  $\bar{t} = 54.22$  s,  $\bar{t} = 112.14$  s, and  $\bar{t} = 112.1$  s respectively.

## 5. EXPERIMENTAL VALIDATION

dire che usi FL-AIR per il drone, pensa se incrementare  $\varepsilon$  a 20cm invece di 17cm e rifare i plot come nelle simulazioni (stelle e XY)

For each obstacle, just add a corrective APF term: [add formula](#)

Increased  $y_A^d$  of 0.5 m, formation reached after 55.30 s(the drone takes some time, but  $R_2$  achieve the formation w.r.t  $R_1$  after 16.02 s), when swapped the formation is achieved after 9.74 s (drone after 8.32 s while  $R_2$  after 9.74 s).



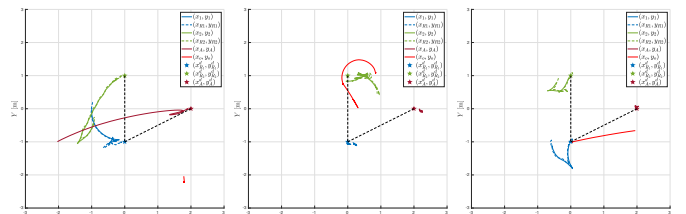
(a)  $R_2$  on the right      (b)  $R_2$  on the left

## 6. CONCLUSION

...

## REFERENCES

- Aditya, P. and Werner, H. (2023). A distributed linear quadratic discrete-time game approach to formation control with collision avoidance. In *2023 62nd IEEE Conference on Decision and Control (CDC)*, 1239–1244. doi:10.1109/CDC49753.2023.10384062.
- Deshpande, P., Menon, P.P., Edwards, C., and Postlethwaite, I. (2011). Formation control of multi-agent systems with double integrator dynamics using delayed static output feedback. In *2011 50th IEEE Conference on Decision and Control and European Control Conference*, 3446–3451. doi:10.1109/CDC.2011.6161074.
- Gattami, A., Bernhardsson, B.M., and Rantzer, A. (2012). Robust team decision theory. *IEEE Transactions on Automatic Control*, 57(3), 794–798. doi:10.1109/TAC.2011.2168071.
- Güler, S. and İsa E. Yıldırım (2023). A distributed relative localization approach for air-ground robot formations with onboard sensing. *Control Engineering Practice*, 135, 105492. doi: <https://doi.org/10.1016/j.conengprac.2023.105492>.
- Han, L., Wang, Y., Yan, Z., Li, X., and Ren, Z. (2024). Event-triggered formation control with obstacle avoidance for multi-agent systems applied to multi-uav formation flying. *Control Engineering Practice*, 153, 106105. doi: <https://doi.org/10.1016/j.conengprac.2024.106105>.
- Huang, F., Duan, M., Su, H., and Zhu, S. (2023). Distributed optimal formation control of second-order multiagent systems with obstacle avoidance.



(a)  $0s \leq t \leq 11s$       (b)  $31s \leq t \leq 42s$       (c)  $56s \leq t \leq 63s$

Fig. 11. TODO

*IEEE Control Systems Letters*, 7, 2647–2652. doi: 10.1109/LCSYS.2023.3287950.

Lee, G. and Chong, N.Y. (2009). Decentralized formation control for small-scale robot teams with anonymity. *Mechatronics*, 19(1), 85–105. doi: <https://doi.org/10.1016/j.mechatronics.2008.06.005>.

Maldonado, D., Cruz, E., Abad Torres, J., Cruz, P.J., and Gamboa Benitez, S.d.P. (2024). Multi-agent systems: A survey about its components, framework and workflow. *IEEE Access*, 12, 80950–80975. doi: 10.1109/ACCESS.2024.3409051.

Morando, A.E.S., Bozzi, A., Zero, E., Sacile, R., and Castillo, P. (2025). Robust control architecture for fleet formation based on lmi and artificial potential fields. In *2025 20th Annual System of Systems Engineering Conference (SoSE)*, 1–6. doi: 10.1109/SoSE66311.2025.11083835.

Piet, B., Strub, G., Changey, S., and Petit, N. (2025). Control of an uav swarm in amorphous formation. In *2025 American Control Conference (ACC)*, 469–475. doi:10.23919/ACC63710.2025.11108054.

Restrepo, E., Loría, A., Sarras, I., and Marzat, J. (2023). Robust consensus of high-order systems under output constraints: Application to rendezvous of underactuated uavs. *IEEE Transactions on Automatic Control*, 68(1), 329–342. doi:10.1109/TAC.2022.3144107.

Semsar-Kazerooni, E. and Khorasani, K. (2009). An lmi approach to optimal consensus seeking in multi-agent systems. In *2009 American Control Conference*, 4519–4524. doi:10.1109/ACC.2009.5160268.

Tran, V.P., Garratt, M.A., and Petersen, I.R. (2021). Multi-vehicle formation control and obstacle avoidance using negative-imaginary systems theory. *IFAC Journal of Systems and Control*, 15, 100117. doi: <https://doi.org/10.1016/j.ifacsc.2020.100117>.

Trejo, J.A.V., Ponsart, J.C., Adam-Medina, M., Valencia-Palomo, G., and Theilliol, D. (2023). Distributed observer-based leader-following consensus control for lpv multi-agent systems: Application to multiple vtol-uavs formation control. In *2023 International Conference on Unmanned Aircraft Systems (ICUAS)*, 1316–1323. doi: 10.1109/ICUAS57906.2023.10156012.

Wang, H., Qiu, T., Liu, Z., Pu, Z., and Yi, J. (2020). Multi-agent formation control with obstacles avoidance under restricted communication through graph reinforcement learning. *IFAC-PapersOnLine*, 53(2), 8150–8156. doi:<https://doi.org/10.1016/j.ifacol.2020.12.2300>. 21st IFAC World Congress.

Yongshen, L., Xuerong, Y., Yajun, Y., and Shengdong, P. (2018). Formation control of ugv's based on artificial potential field. In *2018 37th Chinese Control Conference (CCC)*, 6830–6835. doi:10.23919/ChiCC.2018.8483701.

Zhong, S., Tian, H., Xia, Y., and Liu, H. (2025). Quadrotor formation maneuver control via reinforcement learning. In *2025 44th Chinese Control Conference (CCC)*, 1–6. doi:10.23919/CCC64809.2025.11179569.